Title

Role of soluble epoxide hydrolase in the abnormal activation of fibroblast-like synoviocytes from patients with rheumatoid arthritis

Authors

Pu, Yaoyu

Cheng, Ruijuan

Zhang, Qiuping

et al.

Publication Date

2023-12-01

DOI

10.1016/j.clim.2023.109850

Peer reviewed

HHS Public Access

Author manuscript

Clin Immunol. Author manuscript; available in PMC 2024 December 01.

Published in final edited form as:

Clin Immunol. 2023 December ; 257: 109850. doi:10.1016/j.clim.2023.109850.

Role of soluble epoxide hydrolase in the abnormal activation of fibroblast-like synoviocytes from patients with rheumatoid arthritis

Yaoyu Pu[1,†], **Ruijuan Cheng**[1,†], **Qiuping Zhang**[1], **Tianwen Huang**[1], **Chenyang Lu**[1], **Zhigang Tang**[1], **Yutong Zhong**[1], **Liang Wu**[1], **Bruce D. Hammock**[2,*], **Kenji Hashimoto**[3,*], **Yubin Luo**[1,*], **Yi Liu**[1,*]

[1]Department of Rheumatology and Immunology, West China Hospital, Sichuan University, Chengdu, Sichuan, 610041, China

[2]Department of Entomology and Nematology and UC Davis Comprehensive Cancer Center, University of California, Davis, CA 95616

[3]Division of Clinical Neuroscience, Chiba University Center for Forensic Mental Health, Chiba 260-8670, Japan

Abstract

Rheumatoid arthritis (RA) is an autoimmune disease characterized by enigmatic pathogenesis. Polyunsaturated fatty acids (PUFAs) are implicated in RA's development and progression, yet their exact mechanisms of influence are not fully understood. Soluble epoxide hydrolase (sEH) is an enzyme that metabolizes anti-inflammatory epoxy fatty acids (EpFAs), derivatives of PUFAs. In this study, we report elevated sEH expression in the joints of CIA (collagen-induced arthritis) rats, concomitant with diminished levels of two significant EpFAs. Additionally, increased sEH expression was detected in both the synovium of CIA rats and in the synovium and fibroblast-like synoviocytes (FLS) of RA patients. The sEH inhibitor TPPU attenuated the migration and invasion capabilities of FLS derived from RA patients and to reduce the secretion of inflammatory factors by these cells. Our findings indicate a pivotal role for sEH in RA pathogenesis and suggest that sEH inhibitors offer a promising new therapeutic strategy for managing RA.

Keywords

Fibroblast-like synoviocytes; Inflammation; Rheumatoid arthritis; Soluble epoxide hydrolase; Synovium

[*]**Correspondence**: Prof. Yi Liu (yi2006liu@163.com), Prof. Yubin Luo (luoyubin2016@163.com), Prof. Bruce D. Hammock (bdhammock@ucdavis.edu) and Prof. Kenji Hashimoto (hashimoto@faculty.chiba-u.jp).

[†]Dr. Pu and Dr. Cheng contributed equally to this work.

Author Contributions: Y.P., B.D.H., K.H., L.Yubin., and L.Yi. designed research; Y.P., R.C., Q.Z., T.H., C.L., Z.T., Y.Z., and L.W., performed research; Y.P. analyzed data; Y.P., B.D.H., and K.H. wrote the paper. All authors approved the final manuscript.

Introduction

Rheumatoid arthritis (RA) is a chronic, progressive autoimmune condition characterized by symptoms of joint pain, swelling, and functional impairment [1]. Epidemiologically, the prevalence of RA fluctuates based on geographical, gender, and age-related factors, with global estimates ranging from 0.5% to 1% [2, 3]. Although advances have been made in the treatment of RA, they remain ineffective for 30–40% of patients [4–7]. The underlying pathogenesis of RA, while not entirely unraveled, is believed to be critically influenced by synovial dysfunction and inflammatory cell infiltration within the joints [8].

Patients with RA show heightened activation of fibroblast-like synoviocytes (FLS) in the synovial tissue, leading to increased proliferation and a propensity for these cells to invade and degrade bone and cartilage [9]. RA-associated FLS produce an array of matrix metalloproteinases (MMPs), including MMP-1, 3, 9, and 13, and pro-inflammatory cytokines such as tumor necrosis factor-α (TNF-α) and interleukin-6 (IL-6), which exacerbate joint matrix breakdown and synovial inflammation, culminating in the joint destruction characteristic of RA patients [10].

In the RA synovium, activated FLS secrete inflammatory mediators like TNF-α and monocyte chemoattractant protein-1 (MCP-1), which facilitate monocyte migration into the joint [11]. The resultant buildup of monocytes and macrophages in the joint tissue exacerbates RA pathology [12, 13]. The presence of M1-polarized macrophages, which release inflammatory factors and chemokines, not only maintains inflammation but also recruits additional immune cells, perpetuating joint damage [14, 15]. The ensuing immune activity within the joints can cause spleen enlargement and increased splenic and circulating T cells, contributing to systemic inflammation and associated extra-articular manifestations in RA, including cardiovascular and pulmonary conditions [16, 17].

Emerging research points to the role of polyunsaturated fatty acids (PUFAs) and their metabolic derivatives in RA pathogenesis [18, 19]. Epoxy fatty acids (EpFAs) are formed from their corresponding polyunsaturated fatty acids by oxidation by cytochrome P450 enzymes. Certain EpFAs, such as epoxyeicosatrienoic acids (EETs) from arachidonic acid (ARA), and particularly the 17,18-epoxyeicosapentaenoic acid epoxide (17,18-EpETE) of the corresponding omega-3 fatty acid eicosapentaenoic acid (EPA) possess potent anti-inflammatory and anti-oxidative abilities. However, these effects are transient as EpFAs are rapidly hydrolyzed by the soluble epoxide hydrolysis (sEH) into the corresponding diols, resulting in the loss of their effects [20]. Elevated sEH expression has been implicated in various psychiatric and neurological disorders, evidenced by its high expression in related brain regions in animal models of depression, schizophrenia, autism spectrum disorder (ASD), and Parkinson’s disease [21–25]. Inhibition of sEH with TPPU has been shown to ameliorate symptoms in these conditions [21–25], as well as improve ASD-like behaviors in offspring following maternal glyphosate exposure [26]. While TPPU has been found to relieve hyperalgesia and edema in the collagen-induced arthritis (CIA) model [27], the precise mechanisms of its therapeutic action in RA are still largely unknown, and its effects on sEH in RA patient samples remain unreported.

The study aims to elucidate the role of sEH in RA pathogenesis and to evaluate the therapeutic potential of the sEH inhibitor TPPU in the condition. First, we investigate sEH expression of CIA rats, a well-established animal model of RA. We assess whether sEH is upregulated in the synovium of these animals and its contribution to synovial dysfunction. Additionally, we explore the elevation of sEH in the synovium and FLS of RA patients. Through cellular studies, we examine the potential of TPPU to mitigate inflammatory factor secretion and impair the migration and invasion of FLS derived from RA patients. We also explore whether TPPU influences macrophage polarization, potentially averting further inflammatory exacerbation. Ultimately, we assess the overall impact of TPPU on joint health and systemic inflammation in CIA rats using flow cytometry, RT-PCR and complete blood counts.

Materials and Methods

Animals and animal care.

Female Wistar rats (8 weeks old, 180–220 g) were purchased from HuaFuKang Co., Ltd. (Beijing, China). Every four rats were housed in clear polycarbonate cages (56 × 35 × 21 cm) under controlled temperature (23 ± 1 °C) and 12-h light/dark cycles (lights on between 07:00–19:00) with libitum food (SPF mice food; Beijing Keao Xieli Feed Co., Ltd., Beijing, China). This study was conducted in strict accordance with the recommendations in the Guide for the Care and Use of Laboratory Animals of the National Institutes of Health, USA. The experimental protocol of this study was approved by the Sichuan University Institutional Animal Care and Use Committee (Permission number 20220414003).

Treatment of CIA and TPPU.

CIA was induced as previously reported [28]. Briefly, female Wistar rats (8 weeks) were randomly divided into two groups and intradermally immunized at a site located 1 cm from the base of the tail with a mixture of bovine type II collagen (CII) (Cat# 20022, Chondrex, WA, USA) and an equal volume of incomplete Freund's adjuvant (IFA) (Cat# 7002, Chondrex, WA, USA), followed by a booster injection of the same mixture 7 days later. The clinical scores of arthritis (0–4) were evaluated from day 14 to 28 after the first immunization, with scores assigned as follows: 0, no swelling; 1, erythema or swelling of finger joints; 2, mild swelling of wrist or ankle joints; 3, severe swelling of whole paws; 4, deformity or ankylosis of paws. The maximum score per rat was 16, calculated by adding the scores of all four paws.

TPPU (Cat#11,120, Cayman Chemical, Ann Arbor, MI, USA) treatment was carried out using the same method as described in a previous report [22]. Briefly, TPPU was in warm polyethylene glycol and added to warm drinking water with stirring to a final concentration of 1% polyethylene glycol 400 (V/V) (PEG 400; Tokyo Chemical Industry Co., Ltd, Tokyo, Japan) to achieve a final concentration of 15 mg/L of TPPU. Drinking water was held at room temperature to prevent crystallization of the TPPU. From day 14 after the first immunization, the rats were provided with either TPPU or vehicle in drinking water for 15 consecutive days until day 28.

Collection of synovium and cell culture.

We collected synovial tissue from RA patients and OA (osteoarthritis) patients who were undergoing knee arthroplasty. RA diagnosis was based on the ACR (American College of Rheumatology)/EULAR (European League Against Rheumatism) 2010 rheumatoid arthritis classification criteria, while OA diagnosis was based on the NICE (National Institute for Health and Care Excellence) 2015 quality standard for osteoarthritis in over 16s. All patients knew and agreed to the use of their tissues for scientific research, and the study procedure was approved by the Biomedical Research Ethics Committee at West China Hospital of Sichuan University (2019610). Sociodemographic factors and clinical symptoms are summarized in Table S1.

The collected synovial tissue was washed three times with PBS, cut into approximately 1 mm^3 pieces, and digested with 0.5mg/ml type VIII collagen at 37°C for 2 hours. After centrifugation at 1,000 rpm for 5 minutes, the pellet was broken up and cultured with complete culture media (CCM) containing 2% penicillin/streptomycin (Cat#15,140,122, Thermo Fisher Scientific, Waltham, MA, USA) and 10% fetal bovine serum (FBS) (Cat#10,091,148, Thermo Fisher Scientific, Waltham, MA, USA) on 25-mm tissue culture Petri dishes (Cat#431,080, Corning, NY, USA) in a standard 5% CO_2 incubator at 37 °C. After three days of incubation in the incubator, the medium was changed and passage 1 (P1) FLS were obtained. The culture media were changed every 3 days, and cells were digested with 0.25% trypsin/EDTA (Cat#25,200,056, Thermo Fisher Scientific, Waltham, MA, USA) for subculture. P3-P9 cells were used for the experiment.

Primary chondrocytes culture and co-culture.

Rat knee cartilage tissue was cut into 1 × 1 × 1 mm pieces and washed with PBS to remove debris. Subsequently, it was treated with a 0.25% trypsin/EDTA for 30 minutes at 37°C to remove impurities. Overnight digestion at 37°C with CCM containing 0.25% type II collagenase was followed, ensuring full submersion of tissue pieces. Chondrocytes were then harvested by centrifugation at 1200 rpm for 5 minutes at 4°C and resuspended in a sterile CCM comprising 2% penicillin/streptomycin and 10% FBS. Chondrocytes were cultured at 37°C with 5% CO_2 in a humidified incubator, as described above. The culture media were changed every 3 days, and cells were digested with 0.25% trypsin/EDTA for subculture. Cells from P3-P9 were used for the experiment, as previously described.

The co-culture system was established as previously reported and performed using a 0.4 μm cell culture insert (Cat#P575–5, Corning, NY, USA) [29]. In brief, primary rat chondrocytes (1×10^5) were allowed to adhere to 24-well plates overnight. The following day, RA FLS were placed in the upper chamber. The RA FLS were co-cultured with rat chondrocytes in a 1:1 ratio at 37°C with 5% CO_2 in a humidified incubator for 72 hours. After this period, the chondrocytes were collected and used for subsequent experiments.

Monocyte culture and macrophage polarization.

The isolation of rat bone marrow-derived macrophages (BMDM) and the induction of polarization were performed as previously reported [30]. After sacrificing the rat, the intact femur and tibia were separated using scissors to remove muscle and other soft tissues.

Under sterile conditions, the leg bone was severed at the joint. A 1 mL syringe filled with RPMI 1640 medium was inserted into the bone marrow cavity and used for repeated rinsing. Then, 10 mL of M-CSF (40 ng/mL) solution was added to the bone marrow rinse, and the mixture was centrifuged at 300 g for 5 minutes. The supernatant was discarded, and the cells were resuspended in 5 mL of 1640 medium containing M-CSF (40 ng/mL) and 10% fetal bovine serum. The solution was then incubated for 7 days. Regarding the induction of polarization in the M1 versus M2 direction, BMDMs were stimulated with 100 ng/ml of lipopolysaccharide (LPS) and 50 ng/ml of interferon-γ (IFN-γ) for 24 hours for M1, while 20 ng/ml of IL-4 was used to induce M2.

The human monocyte cell line THP-1 was obtained from BLUEFBIOTM Biotechnology Development Co., Ltd. (BFN60700157, Shanghai, China). Cell line authentication was performed using short tandem repeat (STR) analysis by the Core Facilities of West China Hospital. THP-1 cells were cultured in RPMI 1640 medium supplemented with 2% penicillin/streptomycin and 10% FBS at 37 °C with 5% CO_2 in a humidified incubator. To induce M0 macrophages, THP-1 cells were treated with 100 ng/mL PMA for 48 hours. After obtaining M0 cells, M1 polarization was induced by adding 100 ng/mL LPS and 20 ng/mL IFN-γ to the culture medium for 24 hours, while M2 polarization was induced by adding 20 ng/mL IL-4 and 20 ng/mL IL-13 for 24 hours. To investigate the effect of TPPU on macrophage polarization, vehicle or different concentrations of TPPU (1, 3, or 10 μg/mL) were added to the culture medium during polarization induction.

Cell viability assay.

To test cell vitality, we used the Cell Counting Kit-8 (CCK-8) in accordance with the manufacturer's instructions. 5×10^3 cells were seeded into the wells of a 96-well plate, followed by the treatment of either vehicle or different concentrations of TPPU 12 hours later. 100 μl of CCK-8 was added to each well at 24 and 48 hours after the treatment. The plate was then incubated at 37°C and 5% CO_2 for 2 hours, and the optical density at 450 nm was measured.

Wound healing assay.

Cell migration was assessed using a wound healing assay. For the wound healing assay, 2×10^5 FLS were seeded into each well of a 6-well plate and cultured until they reached 90% area of the plate. The cells were then starved overnight in serum-free medium before a straight wound was created using a 10 μl pipette tip. After washing away cell debris with medium, the cells were treated with vehicle or different concentrations of TPPU in medium containing 1% FBS to minimize cell proliferation. The wound gap was photographed at 0, 6, 12, 18, and 24 hours, and the area of the cellular wound was measured using the Wound Healing Size tool in ImageJ [31]. The assay was performed three times independently.

Transwell assay.

Cell invasion was assessed using a transwell assay with 8 μm pore size transwell chambers (Corning Incorporated, Corning, NY, USA). Initially, 5×10^4 cells were resuspended in serum-free medium, seeded into the upper chamber of the transwell, while the lower chamber was filled with either a vehicle or different concentrations of TPPU in complete

medium. Following 24 hours of incubation, the cells in the upper chamber were carefully removed using a cotton swab, and the cells that had migrated across the membrane to the lower surface were fixed using 4% paraformaldehyde and stained with 0.1% crystal violet. Five random fields of view were selected under a microscope, and the number of cells was counted.

Immunohistochemistry and immunofluorescence.

Immunohistochemistry (IHC) and immunofluorescence (IF) were performed as previously described [32]. Fresh joint tissues were fixed in 4% paraformaldehyde in 0.1 M phosphate buffer (pH 7.4) for 48 hours, then dehydrated, and embedded in paraffin. Tissue sections were cut to 4 μm. Next, tissue sections were heated at 65°C for 2 hours and treated with a sequence of xylene and alcohol for deparaffinization. Antigen retrieval was performed by heating the sections to 95°C with SignalStain® Citrate Unmasking Solution (Cat#14,746, Cell Signaling Technology, Boston, MA, USA). The sections were then washed three times with 0.05 M Tris–HCl saline (TBS) with 0.1% Tween-20 (TBST). For IHC, tissue sections were incubated in 3% H_2O_2 in TBST for 30 minutes and blocked with 5% goat serum in TBST for 1 hour at room temperature. The samples were then incubated with anti-sEH antibody (Cat#DF6676. 1:500, Affinity Bioscience) overnight at 4°C, followed by incubation with goat anti-rabbit IgG(H+L) (1:10,000, Cat#AS070, Abconal, Woburn, MA, USA) for 1 hour at room temperature. The sections were then reacted with DAB for 5 minutes and washed three times. The sections were mounted on gelatinized slides, dehydrated, cleared, and coverslipped under Permount® (Fisher Scientific, Fair Lawn, NJ, USA). Images were automatically scanned by a Vectra Polaris Automated Quantitative Pathology Imaging System (PerkinElmer, Waltham, MA, USA).

For IF, the cell sections were prepared by co-incubating 2×10^4 cells with glass slides. After fixing with 4% paraformaldehyde for 15 minutes and permeabilizing with 0.5% Triton X-100 at room temperature for 20 minutes, the cell slides were blocked as described above. Cell slides were then incubated with anti-sEH antibody (Cat# DF6676. 1:500, Affinity Bioscience), anti-collagen II antibody (Cat# AF0135. 1:200, Affinity Bioscience) and anti-SOX9 antibody (Cat# AF6330. 1:500, Affinity Bioscience) separately for 24 hours at 4 ℃, followed by incubation with goat anti-rabbit Alexa Fluor 488 antibody (1:500, Cat# 4412, Cell Signaling Technology, Danvers, MA, USA) for 1 hour at room temperature in the dark. After three washes with TBST, the sections were mounted using mounting medium with DAPI (Cat# S2110, Solarbio, Beijing, China). The cell slides were then automatically scanned as described above.

Western blot analysis.

Western blot analysis was conducted following previously reported methods [33]. Approximately 5×10^5 cells treated with either vehicle or TPPU were lysed with 100 μl of SDS-PAGA sample loading buffer, heated for 10 minutes at 95°C, and then frozen at − 80°C for later use. To prepare joint tissue for analysis, it was first ground into a powder using a mortar under liquid nitrogen, and then homogenized in Laemmli analysis buffer. Protein concentration was determined using a BCA protein assay kit (Beyotime, Shanghai, China), and 50 micrograms of protein was mixed with

a quarter volume of SDS-PAGE sample loading buffer and heated for 10 minutes at 95°C. The proteins from both the joint tissue and FLS were separated by sodium dodecyl sulfate–polyacrylamide gel electrophoresis using 4–12% FuturePAGETM gels (Cat# ET15412LGel, ACE Biotechnology, Nanjing, China). Proteins were transferred to polyvinylidene difluoride (PVDF) membranes using a Trans-Blot Mini Cell (Bio-Rad). For immunodetection, the blots were blocked with 5% BSA in TBST (TBS + 0.1% Tween-20) for 1 h at room temperature (RT) and incubated with primary antibodies against sEH (Cat#ab155280. 1:10,000, Abcam), PI3K (Cat#AF6241. 1:500, Affinity Bioscience), p-PI3K (Cat#AF3241. 1:2,000, Affinity Bioscience), AKT (Cat#AF6261. 1:500, Affinity Bioscience), p-AKT (Cat#AF0016. 1:2,000, Affinity Bioscience), p65 (Cat#AF5006. 1:500, Affinity Bioscience), p-p65 (Cat#AF2006. 1:2,000, Affinity Bioscience), IkB alpha (Cat#ab32518. 1:10,000, Abcam), p-IkB alpha (Cat#ab133462. 1:10,000, Abcam), p38 (Cat#AF6456. 1:500, Affinity Bioscience), p-p38 (Cat#AF4001. 1:2,000, Affinity Bioscience), JNK (Cat#AF4001. 1:500, Affinity Bioscience), p-JNK (Cat#AF3318. 1:2,000, Affinity Bioscience), ERK (Cat#AF0155. 1:500, Affinity Bioscience), p-ERK (Cat#AF4001. 1:2,000, Affinity Bioscience) and β-actin (Cat#AC026. 1:100,000, ABclonal) separately at 4℃ overnight. The following day, the membranes were washed three times with TBST and then incubated with goat anti-rabbit IgG(H+L) (Cat#AS070, 1:10,000 dilution, ABclonal) for 1 hour at room temperature. After another three washes, the protein bands were detected using a Western Blotting Detection System (GE Healthcare Bioscience) and visualized using a ChemiDoc™ Touch Imaging System (Bio-Rad Laboratories, Hercules, CA). Image analysis was performed using Image LabTM 3.0 software (Bio-Rad Laboratories).

Gene expression analysis by quantitative real-time PCR.

Reverse transcription PCR (RT-PCR) was performed as previously reported [28, 32]. Briefly, 1 mL TRizol was added to joint powder or cells treated with either vehicle or TPPU, mixed well, and left to stand at room temperature for 10 minutes. Then, 200 μL of chloroform was added, vortexed for 15 seconds, and centrifuged at 12,700 RPM and 4°C for 15 minutes. The supernatant was collected and mixed with an equal volume of isopropanol. After a 10-minute reaction, the mixture was centrifuged again at 12,700 RPM and 4°C for 10 minutes. The supernatant was discarded, and the pellet was washed with 75% alcohol (DEPC water) and centrifuged at 12,700 RPM and 4°C for 5 minutes. The supernatant was discarded again, and the precipitate was air-dried at room temperature. Next, 100 μL of DEPC water was added to the sediment to obtain total RNA. The purity of the total RNA was assessed using Nanodrop (Eppendorf, Hamburg, Germany). The RNA samples were then used for first strand cDNA synthesis with All-In-One 5X RT MasterMix (Cat# G592, Applied Biological Materials, Richmond, BC, Canada). All samples were tested in duplicate, and average values were used for quantification. Detailed RNA primers can be found in Table S2.

Flow cytometry.

Flow cytometry analysis was performed as previously reported [28]. For the analysis, trypsinized and centrifuged cells were used directly. Spleens were mashed and passed through a 70 μm mesh to obtain a single-cell suspension, which was then processed by red blood cell lysate buffer and used for staining. To extract rat peritoneal macrophages, a small opening was made in the peritoneal cavity of rats that had been

euthanized with an excess of pentobarbital sodium. The cavity was then repeatedly rinsed using 15 ml of PBS, and the fluid was collected for flow cytometry analysis. To quantify spleen and peritoneal macrophages and bone marrow-derived macrophages, the following antibodies were used: anti-CD11b, FITC (Cat#201805. Biolegend), anti-CD68, PE-Cyanine7 (Cat#201003. Biolegend), anti-CD86, APC (Cat#200315. Biolegend), and anti-CD163, PE (Cat#755542. BD Biosciences). To quantify Thp-1 macrophages, the following antibodies were used: anti-CD11b, FITC (Cat#101205. Biolegend), anti-CD68, PE-Cyanine7 (Cat# 25-0689-42. Invitrogen), anti-CD80, APC (Cat#305220. Biolegend), and anti-CD206, PE (Cat#321106. Biolegend). For regulatory T cell quantification, the following antibodies were used: anti-CD3e, FITC (Cat#11-0030-81. Invitrogen), anti-CD4, PerCP-Cy5.5 (Cat#201519. Biolegend), anti-CD25, APC (Cat#202113. Biolegend), and anti-FOXP3, PE (Cat#12-5773-82. Invitrogen). To analyze Th1/Th2/Th17 cell subsets, around 1×10^6 cells were stimulated with phorbol myristate acetate (50 ng/ml), ionomycin (1 μg/ml), and golgi inhibitor (Cat#51–2301kz, 1:1000, BD GolgiPlug) and then harvested and stained with the following antibodies: anti-IFN-γ, Alexa Fluor® 647 (Cat#507810. BioLegend), anti-IL-17A, eFluor™ 450 (Cat# 48-7177-80, Invitrogen), anti-IL-4, PE (Cat#511905. BioLegend), and anti-CD3e and CD4 antibodies as described above. A BD FACSCalibur flow cytometer (BD Biosciences) was used to detect cells, and the data were analyzed using FlowJo software (Version 7.6.1).

Oxylipin analysis.

The analysis of oxylipins was conducted by Wuhan Metware Biotechnology Co., Ltd (Wuhan, China). Briefly, 20 mg of joint grinding powder was mixed with 200 μl of methanol using a homogenizer, then vortexed for 5 minutes and left at a low temperature to precipitate proteins. A 1 μM internal standard mix (20 μl) was added to each sample, vortexed for 5 minutes, and then centrifuged at 5,000 rpm for 10 minutes at 4°C. The supernatant was collected, dried in nitrogen, and the resulting powder was dissolved in 10% methanol and adjusted the pH to 3.5. The sample was then passed through a solid-phase extraction column, and elution was performed using 10 mL of methyl formate. The eluates were collected, dried in nitrogen, and reconstituted with 100 μL methanol/water (v:v = 1:1). The supernatants were analyzed by ExionLC™AD and QTRAP®6500+ and the data were analyzed by Analyst 1.6.3 Software.

Micro-computed tomography.

Micro-computed tomography (Micro-CT) imaging was conducted using the Quantum GX micro-CT imaging system (PerkinElmer, USA). The system was configured with optimized parameters for visualizing calcified tissues, employing a voltage of 90 kV and a current of 88 μA, resulting in a pixel size of 100 μm. Three-dimensional images of rat paws were acquired and stored in the Rigaku Database. To assess the bone structure, focus was directed towards the tibia within the right knee joint. The analysis commenced from a specific anatomical reference point situated at the growth plate. The assessment extended distally for a span of 2 mm, encompassing 40 sequential tomograms. To segment the 3D volumes of the tibia, an evaluation script employing adjusted grayscale thresholds from the Caliper Micro-CT analysis tools was employed. Quantitative analysis was carried out using two key parameters: Bone Surface per Total Volume (BS/TV) and Trabecular Number (TB.N).

Complete blood count.

The blood routine of rat blood was analyzed and detected by Mindray CAL8000 at Chengdu ADICON Clinical Laboratories.

Statistical analysis.

All statistical analyses were performed using R V.4.1.3. Animal and cell experimental data were presented as the mean ± standard error of the mean (S.E.M.). The data of body weight, clinical score and wound healing assay were analyzed using repeated measure one-way analysis of variance (ANOVA), followed by post hoc Tukey's multiple comparison tests. The results of western blotting, RT-PCR, oxylipin analysis, CCK-8, transwell migration assay and flow cytometry were analyzed by Student's t-test (for two groups) or one-way ANOVA, followed by post hoc Tukey's multiple comparison tests (for multiple groups). RT-PCR and flow cytometry results regarding the therapeutic effect of TPPU on CIA rats were analyzed using two-way ANOVA and post hoc Tukey's multiple comparison tests. *P* values of less than 0.05 were considered statistically significant.

Results

Increased expression of sEH in the synovium of CIA rats.

First, we created CIA rat models, and collected the blood and joint samples 4 weeks after the first injection (Fig. 1A). The comparative body weight of CIA rats was significantly below that of controls from day 14 compared to the control group (Fig. 1B). From day 7, the joints of CIA rats gradually turned red and swollen, with increased clinical scores (Fig. 1C). Histological analysis of the joints by H&E staining revealed infiltration, thickening of the synovial membrane, and disappearance of lipids in CIA rats (Fig. 1D). Toluidine blue and Masson's trichrome staining showed severe cartilage and bone destruction in CIA rats (Fig. S1). Moreover, RT-PCR results exhibited an increased expression of TNF-α, IL-1β, IL-6, MMP-1, MMP-3, MMP-9, and MMP-13 in CIA rat joints (Fig. S2).

Next, we assessed the expression of sEH in the joints of both control and CIA rats. Protein levels of sEH in the joints of CIA rats were significantly elevated compared to control rats (Fig. 1E). Furthermore, gene expression of sEH (also known as *Ephx2*) mRNA in the joints of CIA rats was significantly higher than that in control rats (Fig. 1F).

Additionally, we conducted oxylipin analysis to measure the levels of eicosanoid metabolites in the joints of rats (Fig. 1G and 1H, Table S3 and S4). Several PUFAs such as eicosapentaenoic acid (EPA), arachidonic acid (ARA), docosahexaenoic acid (DHA), dihomo-γ-linoleic acid (DGLA), and γ-linoleic acid (GLA) were significantly increased in the synovial tissues of CIA rats compared to control rats (Table S3). Furthermore, we observed decreased levels of 9,10-EpOME [9,10-epoxy-12Z-octadecenoic acid] and 17,18-EpETE [17,18-epoxy-5Z,8Z,11Z,14Z-eicosatetraenoic acid] in the CIA rats compared to control rats although their corresponding diols were not different between the two groups (Fig. 1G and 1H). Moreover, the expressions of sEH and the *Ephx2* mRNA were negatively correlated with 9,10-EpOME and 17,18-EpETE (Fig. S3). In contrast, levels of 5,6-EpETrE

[5,6-epoxy-8Z,11Z,14Z-eicosatrienoic acid] were significantly increased in CIA rats (Table S3).

Lastly, we performed immunohistochemistry analysis for sEH in joint sections of control and CIA rats. We observed increased expression of sEH primarily in the synovial tissue (Fig. 1I), rather than in bone, cartilage, bone marrow, and muscle of CIA rats (Fig. S4).

Increased expression of sEH in the synovial tissue and in fibroblast-like synoviocytes from RA patients.

To support our findings on increased sEH expression in synovial tissue from CIA rats, we collected synovial tissue from RA and OA (osteoarthritis) patients undergoing joint arthroplasty, with OA patients as controls. Immunohistochemistry demonstrated that the sEH expression in the synovial tissue from RA patients significantly increased compared to OA patients (Fig. 2A). We further isolated and cultured FLS from the synovial tissue of RA and OA patients, as FLS play a crucial role in the pathogenesis of RA. Western blot and RT-PCR analyses revealed higher sEH expression in the FLS from RA patients compared to FLS from OA patients (Fig. 2B). Immunofluorescence analysis also showed higher fluorescence intensity in the FLS from RA patients compared to the FLS from OA patients (Fig. 2C). Collectively, these data suggest elevated sEH expression in the RA FLS from RA patients compared to FLA from OA patients.

Effects of TPPU on migration, invasion, and pro-inflammatory cytokine release of FLS from RA patients.

We used TNF-α to mimic the inflammatory environment of RA. Under this condition, FLS exhibited accelerated proliferation and strong invasion, leading to synovial hyperplasia, as well as bone and cartilage erosion. In addition, we used the sEH inhibitor TPPU to assess the role of sEH on the abnormal functions of FLS from RA patients. Cell viability was assessed using a CCK-8 (cell counting kit-8) assay after treating FLS with various concentrations of TPPU. TPPU at concentrations higher than 60 μg/ml occasionally resulted in crystal precipitation in the cell culture medium under our experimental conditions. Therefore, the highest concentration of TPPU used in this study was 60 μg/ml, which did not impact FLS viability (Fig. 2D). Cell migration tests used as indicators of wound healing were performed using TPPU at concentrations of 3, 10, and 30 μg/ml. Treatment with 30 μg/ml TPPU significantly reduced the migration ability of FLS from RA patients (Fig. 2E). Additionally, 10 μg/ml and 30 μg/ml TPPU significantly decreased cell invasion of RA FLS as tested by transwell assay (Fig. S5). Moreover, TPPU (3, 10, or 30 μg/ml) attenuated the increased expressions of *Ephx2*, *Il6*, *Mmp1*, *Mmp3*, *Mmp9*, and *Mmp13* mRNAs in the FLS treated with TNF-α, in a concentration manner (Fig. S6). Western blot analysis showed that TPPU (30 μg/ml) significantly ameliorated the elevated levels of p-p65/p95 in the FLS treated with TNF-α, suggesting stabilization of p65 protein and inhibition of the NF-κB signaling pathway in the activation of FLS from RA patients (Fig. 2F). In contrast, TPPU (30 μg/ml) had no effect on the P38/JNK/ERK MAPK signaling pathways and PI3K-AKT signaling pathways, which are involved in the FLS activation from RA patients [34, 35] (Fig. S7).

Inhibition of sEH suppressed Thp-1 monocyte differentiation to macrophages and polarization to M1 macrophages.

Macrophages play a crucial role in the development and progression of RA as the main source of multiple inflammatory cytokines [36–38]. Here, we conducted CCK-8 tests to evaluate the effect of TPPU on the viability of Thp-1, a human monocytic cell line. Unlike FLS, TPPU (60 μg/ml and 30 μg/ml) showed cytotoxic effects on Thp-1 cells within 48 hours (Fig. 3A). Therefore, we used TPPU at concentrations no more than 10 μg/ml in our experiments. RT-PCR was used to detect markers of Thp-1-induced macrophages, and the results revealed that TPPU significantly decreased the expression of M1 macrophage markers such as CD80, CD86, and IL-12p40, while it had no impact on the expression of M2 macrophage markers such as CD206, CD163, and Fizz-1 (Fig. 3B and Fig. S8A). Flow cytometry analysis showed that TPPU inhibited the differentiation of Thp-1 monocytes into macrophages and the polarization towards M1 macrophages, without affecting polarization towards M2 macrophages (Fig. 3C and Fig. S8B). To corroborate our findings, we harvested and cultured BMDMs from rats to examine macrophage polarization. TPPU at a concentration of 10 μg/ml had no detrimental effect on the viability of BMDM cells (Fig. S9A). Flow cytometry results revealed that TPPU significantly suppressed the shift of BMDMs to an M1 phenotype without affecting the M2 macrophage polarization (Fig. S9B and C). These results were consistent with the findings in THP-1 cell studies. These findings suggest that TPPU may have a beneficial role in RA by inhibiting monocyte colonization and differentiation in the joint, as well as M1 polarization, all of which are associated with propagation of inflammation.

Effects of TPPU on joint swelling and suppression of T cell immunity in spleen and blood of CIA rats.

One week after the second injection of the mixture of collagen and incomplete Freund's adjuvant, the rats were provided with either vehicle or TPPU at a concentration of 15 mg/L in their drinking water to investigate the effects of TPPU on CIA rats (Fig. 4A). Although TPPU did not have any effects on the body weight of the CIA rats, it alleviated joint redness and swelling, as well as decreased the clinical score (Fig. 4B and C). H&E staining revealed that TPPU decreased the infiltration of inflammatory cells in the joints and reduced cartilage and bone destruction in CIA rats (Fig. 4D). Micro-CT analysis of rat tibiae revealed the protective effects of TPPU against bone erosion attributable to CIA (fig. S10A). TPPU was found to increase the Bone Surface to Total Volume (BS/TV) ratio as well as the Trabecular Number (TB.N) (Fig. S10B) (Fig. S10A and B). Building on the Micro-CT findings, we further developed a co-culture system of RA FLS with rat primary chondrocytes. The results indicated that the co-culturing these cell types significantly diminished the expression of SOX9 and COL2A1 in the chondrocytes, an effect that was notably reversed by TPPU (Fig. S10C). Immunofluorescence staining for chondrocytes for collagen type II (COL Ⅱ) and SOX9 revealed that TPPU substantially countered the downregulation of collagen type II caused by RA FLS co-culture (Fig. S10C). Immunofluorescence staining of chondrocytes for collagen type II (COL Ⅱ) and SOX9 revealed that TPPU substantially countered the downregulation of collagen type II caused by RA FLS co-culture (Fig. S10D). Flow cytometry showed that TPPU decreased the increased numbers of T cells in the spleen and blood (Fig. 4E). Moreover, TPPU increased the number of Treg cells, and decreased

the proportion of Th17 cells (Fig. 4F and Fig. S11A). However, TPPU did not have any effects on the Th1/Th2 ratio (Fig. S11B). Furthermore, upon analyzing macrophages from the spleen and peritoneal cavity of rats, it was observed that TPPU significantly decreased the expression of M1 macrophages in both splenic and peritoneal environments without affecting the M2 macrophage population (Fig. S12). These outcomes align with those from *in vitro* experiments conducted with bone marrow-derived macrophages and THP-1 cells. Additionally, TPPU significantly ameliorated the increased gene expression of *Ephx2*, *Tnfa*, *Il6*, *Mmp1*, *Mmp3*, *Mmp9*, and *Mmp13* mRNAs in the joints of CIA rats (Fig. S13). Finally, complete blood count analysis revealed that white blood cells, neutrophils, lymphocytes, and monocytes in the blood of CIA rats were increased significantly compared to control group, and TPPU significantly blocked these increases in CIA rats, resulting in suppression of CIA-induced systemic immune activation (Fig. S14).

Discussion

The key findings of the present study are summarized as follows. First, we noted an upregulation of sEH expression in the synovial tissues of CIA rats, with this increase predominantly localized to the synovial tissue rather than other tissues such as bone marrow, muscle, bone, or cartilage. Oxylipin profiling indicated reduced levels of two major EpFAs (9,10-EpOME and 17,18-EpETE) in the joints of CIA rats. Notably, sEH expression was elevated in both synovial tissue and FLS from RA patients in comparison to OA patients. Upon administration the sEH inhibitor TPPU, there was a notable decrease in the release of inflammatory mediators and a reduction in the migratory and invasive behaviors of FLS. TPPU also suppressed FLS activation in RA patients via the NF-κB signaling pathway. Moreover, while TPPU impeded the polarization of macrophages towards the M1 phenotype, it did not alter polarization towards the M2 phenotype. In addition, TPPU was observed to mitigate CIA-induced bone damage and to promote collagen type II expression in chondrocytes after co-culturing with RA FLS. *In vivo*, TPPU was effective in reducing joint swelling and modulating T cell immunity in CIA rats, evidenced by an increase in regulatory T cell expression and a decrease in Th17 cell expression. Among the outcomes, the inhibition of FLS activation in RA patients was particularly distinct and may have the potential to prevent the onset of RA. Collectively, these findings imply a pivotal role for sEH in the pathogenesis of RA and position sEH inhibitors as promising candidates for RA therapy.

In our study, we noted an upregulation of sEH expression in synovial tissues from CIA rats, as well as in synovial tissues and FLS from RA patients. Significantly, treatment with TPPU decreased sEH expression in FLS from RA patients and mitigated their invasive and migratory capabilities, alongside their secretion of inflammatory mediators. Dysfunctional FLS are acknowledged as a critical pathological element in RA, where various factors such as genetics, environmental influences, and trauma may induce aberrant FLS proliferation and activation [39–41]. Consequently, it is plausible that these activated FLS contribute to increased joint vascularization, pannus formation, and the release of self-antigens such as citrullinated proteins, heat shock proteins, and joint-specific antigens, precipitating a sustained influx of inflammatory cells into the joint space [42–44]. This activity constitutes a fundamental distinction between RA and OA patients.

Methotrexate, the standard first-line treatment for RA, has been reported to halt the proliferation cycle of FLS in the G1 stage, thus inhibiting their proliferation [45]. Conversely, sulfasalazine has been demonstrated to suppress the activation of astrocytes and can be used to relieve pain in rats [46]. In this study, while high concentrations of TPPU did not impact the proliferation of FLS from RA patients, they did inhibit the cell's migratory and invasive properties. Although previous research has indicated that TPPU can inhibit the proliferation and migration of vascular smooth muscle cells [47], it has also been reported to enhance the migration of human gingival epithelial cells and human umbilical vein endothelial cells [48]. The effects of TPPU on cell migration are evidently complex and may vary, potentially due to differences in cell types and experimental conditions. This warrants further investigation to fully elucidate the underlying mechanisms.

In this study, we observed that TPPU stabilized p65, consequently inhibiting the downstream NF-κB signaling pathway and mitigating the abnormal activation of FLS. However, TPPU appeared to exert no effect on the PI3K-AKT and MAPK signaling pathways. In both human neuroblastoma cells (SH-SY5Y) and human renal proximal tubule epithelial cells (HK-2), TPPU was found to inhibit NF-κB activation and reduce the release of inflammatory factors, as indicated by previous studies [49, 50]. Additionally, TPPU has been shown to alleviate symptoms in animal models of Alzheimer's disease, depression, diabetes, and other conditions [21, 51–53], with these beneficial effects largely attributed to TPPU's capacity to diminish sEH activity, thereby elevating levels of EpFAs, which are known for their potent anti-inflammatory properties [54, 55]. In the joints of CIA rats, we noted concentrations of 9,10-EpOME (from linoleic acid) and 17,18-EpETE (from EPA). This observation is consistent with the increased expression of sEH in the tissue, as both compounds are recognized as excellent sEH substrates. Interestingly, levels of 9,10-DiHOME, sEH-derived diol of linoleic acid, did not differ between the two groups. This is notable given that 9,10-DiHOME is not predominantly anti-inflammatory; in fact, it is toxic and pro-inflammatory in multiple organ systems, potentially due to the abundance of linoleate in many human diets [56, 57]. Furthermore, it has been reported that supplementation with 9,10-DiHOME can inhibit CD3-induced T cell apoptosis, whereas 17,18-EpETE can bind to G protein-coupled receptors and suppressed hypersensitivity reactions [57, 58]. In stark contrast to expectations, we found elevated levels of 5,6-EpETrE in CIA rats despite increased expression of sEH, which supports the notion that 5,6-epoxides, such as 5,6-EpETrE, are poor substrates for sEH [59]. Moreover, studies have suggested that 17,18-EpETE can suppress the release of TNF-α, IL-6, and IL-8 from human airway epithelial cells, thus attenuating lung inflammation [60, 61]. These findings underscore the need for further research into the interplay between EpFAs and sEH in the metabolisms of PUFAs.

In this study, we discovered that TPPU effectively inhibited the differentiation of THP-1 cells into macrophages and further suppressed their polarization towards the M1 phenotypes. M1 macrophages are recognized as a significant source of inflammatory cytokines, including TNF-α, IL-1β, and IL-6, which play crucial role in the pathogenesis of RA [62, 63]. Previous research has shown that TPPU ameliorates sepsis, which is induced by cecal ligation and puncture, by enhancing macrophage phagocytosis and attenuating the inflammatory response [64]. Additionally, sEH inhibition has been linked to macrophage inactivation, leading to amelioration of acute lung injury caused by LPS [65]. However, the

exact mechanisms by which TPPU affects macrophage differentiation and polarization have yet to be fully elucidated, necessitating further investigation.

Additionally, our findings indicate that TPPU significantly reduced joint swelling in CIA while increasing the proportion of Treg cells, decreasing the proportion of Th17 cells, and dampening T cell-mediated immunity. Treg cells are known to suppress inflammation, whereas Th17 cells are implicated in promoting inflammation across multiple disease states. Consequently, the dynamic equilibrium between these two types of cells is frequently disrupted during disease progression [66–68]. Corroborating our flow cytometry data, a previous study reported that TPPU upregulates the expression of Foxp3 gene and downregulates the expression of the IL-17A gene in CIA mice [27]. Moreover, sEH inhibitors have been shown to decrease Th2-specific cytokines and chemokines, thus reducing airway hyperresponsiveness [69]. Despite these insights, the research exploring the interplay between sEH inhibitors and T cell immunity remains sparse. Therefore, additional research is necessary to clarify the effects and underlying mechanisms of TPPU and other sEH inhibitors on T cells.

In our investigation, we found that TPPU effectively inhibited the polarization of macrophages towards the M1 phenotype without notably affecting M2 macrophage polarization. M1 macrophages are recognized for their pro-inflammatory role, characterized by the secretion of cytokines like IL-1β, IL-6, and TNF-α, which amplify inflammatory responses. In an *in vitro* sepsis model employing RAW264.7 cells stimulated by lipopolysaccharide, TPPU markedly reduced the levels of inflammatory cytokines and simultaneously increased the phagocytic activity of macrophages. This was linked to suppression of the MAPK signaling pathway. Additionally, research has shown that TPPU increases the presence of M2 microglia in the corpus callosum of mice experiencing carotid artery stenosis, as well as in those with cerebral hemorrhage. This elevation in M2 microglia correlates with a therapeutic influence on these conditions. However, the exact signaling pathways and mechanisms by which TPPU influences macrophage polarization remain to be fully elucidated.

In relation to dietary factors and RA, a prospective cohort study showed that dietary intake of n-3 PUFAs in women correlated with a decreased risk of RA onset [73], highlighting the potential influence of PUFA metabolism in the disease's development and progression. Given the clinical progression of sEH inhibitors, such as EC5026 [74], it becomes particularly pertinent to examine whether these inhibitors could ameliorate symptoms in patients with RA.

In conclusion, the data of this study have uncovered that the upregulation of sEH in the synovium plays a pivotal role in the pathogenesis of RA. Furthermore, we have demonstrated that the sEH inhibitor TPPU effectively ameliorates RA by dampening immune responses within the synovium, as well as in macrophages and T cells. Ultimately, this study positions sEH as a promising novel therapeutic target for RA.

Supplementary Material

Refer to Web version on PubMed Central for supplementary material.

Acknowledgements

This study was supported by National Natural Science Foundation of China (to Y. Pu, NO. 82101616), Post-Doctor Research Project, West China Hospital, Sichuan University (to Y. Pu, NO.2021HXBH046), Natural Science Foundation of Sichuan Province (to Y. Pu, NO. NO. 2023NSFSC1703 and to R. Cheng, NO. 2023NSFSC1752), 1·3·5 project for disciplines of excellence, West China Hospital, Sichuan University (to Y. Liu, No. ZYGD18015 and No. ZYJC18003), and NIH/National Institute of Environmental Health Sciences (NIEHS) Grant R35 ES030443-01 (RIVER Award) (to B.D.H.) and NIH/NIEHS Superfund Program Grant P42 ES004699 (to B.D.H.).

B.D.H works with EicOsis on the development of epoxide hydrolase inhibitors for clinical use. The other authors report no competing financial interest.

Abbreviations:

RA	rheumatoid arthritis
FLS	fibroblast-like synoviocytes
sEH	soluble epoxide hydrolase
PUFAs	Polyunsaturated fatty acids
EpFAs	epoxy fatty acids
CIA	collagen-induced arthritis
MMPs	matrix metalloproteinases
TNF-α	tumor necrosis factor-α
IL-6	interleukin-6
MCP-1	monocyte chemoattractant protein-1
EETs	epoxyeicosatrienoic acids
EPA	eicosapentaenoic acid
ASD	autism spectrum disorder
OA	osteoarthritis
CCM	complete culture media
LPS	lipopolysaccharide
IFN-γ	interferon-γ
ARA	arachidonic acid
DHA	docosahexaenoic acid
DGLA	dihomo-γ-linoleic acid

GLA	γ-linoleic acid
9,10-EpOME	9,10-epoxy-12Z-octadecenoic acid
17,18-EpETE	17,18-epoxy-5Z,8Z,11Z,14Z-eicosatetraenoic acid
5,6-EpETrE	5,6-epoxy-8Z,11Z,14Z-eicosatrienoic acid
CCK-8	cell counting kit-8
BMDM	bone marrow-derived macrophages

References

[1]. Smolen JS, Aletaha D, McInnes IB. Rheumatoid arthritis. Lancet 2016;388:2023–38. [PubMed: 27156434]

[2]. Silman AJ, Pearson JE. Epidemiology and genetics of rheumatoid arthritis. Arthritis Res 2002;4 Suppl 3:S265–72. [PubMed: 12110146]

[3]. Carmona L, Villaverde V, Hernández-García C, Ballina J, Gabriel R, Laffon A, et al. The prevalence of rheumatoid arthritis in the general population of Spain. Rheumatology 2002;41:88–95. [PubMed: 11792885]

[4]. Maciejewski M, Sands C, Nair N, Ling S, Verstappen S, Hyrich K, et al. Prediction of response of methotrexate in patients with rheumatoid arthritis using serum lipidomics. Scientific Reports 2021;11:7266. [PubMed: 33790392]

[5]. de Hair MJH, Jacobs JWG, Schoneveld JLM, van Laar JM. Difficult-to-treat rheumatoid arthritis: an area of unmet clinical need. Rheumatology 2017;57:1135–44.

[6]. Fatani AZ, Bugshan NA, AlSayyad HM, Shafei MA, Hariri NM, Alrashid LT, et al. Causes of the Failure of Biological Therapy at a Tertiary Center: A Cross-Sectional Retrospective Study. Cureus 2021;13:e18253. [PubMed: 34712530]

[7]. Radu AF, Bungau SG. Management of Rheumatoid Arthritis: An Overview. Cells 2021;10. [PubMed: 35011571]

[8]. Huber LC, Distler O, Tarner I, Gay RE, Gay S, Pap T. Synovial fibroblasts: key players in rheumatoid arthritis. Rheumatology 2006;45:669–75. [PubMed: 16567358]

[9]. Bartok B, Firestein GS. Fibroblast-like synoviocytes: key effector cells in rheumatoid arthritis. Immunol Rev 2010;233:233–55. [PubMed: 20193003]

[10]. Németh T, Nagy G, Pap T. Synovial fibroblasts as potential drug targets in rheumatoid arthritis, where do we stand and where shall we go? Annals of the Rheumatic Diseases 2022;81:1055–64. [PubMed: 35715191]

[11]. Køster D, Egedal JH, Lomholt S, Hvid M, Jakobsen MR, Müller-Ladner U, et al. Phenotypic and functional characterization of synovial fluid-derived fibroblast-like synoviocytes in rheumatoid arthritis. Scientific Reports 2021;11:22168. [PubMed: 34772990]

[12]. Kurowska W, Kuca-Warnawin E, Radzikowska A, Jakubaszek M, Maślińska M, Kwiatkowska B, et al. Monocyte-related biomarkers of rheumatoid arthritis development in undifferentiated arthritis patients - a pilot study. Reumatologia 2018;56:10–6. [PubMed: 29686437]

[13]. Rana AK, Li Y, Dang Q, Yang F. Monocytes in rheumatoid arthritis: Circulating precursors of macrophages and osteoclasts and, their heterogeneity and plasticity role in RA pathogenesis. Int Immunopharmacol 2018;65:348–59. [PubMed: 30366278]

[14]. Tardito S, Martinelli G, Soldano S, Paolino S, Pacini G, Patane M, et al. Macrophage M1/M2 polarization and rheumatoid arthritis: A systematic review. Autoimmun Rev 2019;18:102397. [PubMed: 31520798]

[15]. Cutolo M, Campitiello R, Gotelli E, Soldano S. The Role of M1/M2 Macrophage Polarization in Rheumatoid Arthritis Synovitis. Front Immunol 2022;13:867260. [PubMed: 35663975]

[16]. El-Waseef D A highlight on CD4(+) T-cells in the spleen in a rat model of rheumatoid arthritis and possible therapeutic effect of omega-3. Histological and Immunofluorescence study. Int Immunopharmacol 2020;81:106283. [PubMed: 32044655]

[17]. Yunt ZX, Solomon JJ. Lung disease in rheumatoid arthritis. Rheum Dis Clin North Am 2015;41:225–36. [PubMed: 25836639]

[18]. Calder PC, Zurier RB. Polyunsaturated fatty acids and rheumatoid arthritis. Curr Opin Clin Nutr Metab Care 2001;4:115–21. [PubMed: 11224655]

[19]. Navarini L, Afeltra A, Gallo Afflitto G, Margiotta DPE. Polyunsaturated fatty acids: any role in rheumatoid arthritis? Lipids Health Dis 2017;16:197. [PubMed: 29017507]

[20]. Morisseau C, Hammock BD. Impact of soluble epoxide hydrolase and epoxyeicosanoids on human health. Annu Rev Pharmacol Toxicol 2013;53:37–58. [PubMed: 23020295]

[21]. Ren Q, Ma M, Ishima T, Morisseau C, Yang J, Wagner KM, et al. Gene deficiency and pharmacological inhibition of soluble epoxide hydrolase confers resilience to repeated social defeat stress. Proceedings of the National Academy of Sciences 2016;113:E1944–E52.

[22]. Ma M, Ren Q, Yang J, Zhang K, Xiong Z, Ishima T, et al. Key role of soluble epoxide hydrolase in the neurodevelopmental disorders of offspring after maternal immune activation. Proceedings of the National Academy of Sciences 2019;116:7083–8.

[23]. Shan J, Hashimoto K. Soluble Epoxide Hydrolase as a Therapeutic Target for Neuropsychiatric Disorders. International Journal of Molecular Sciences 2022;23:4951. [PubMed: 35563342]

[24]. Zhang J, Tan Y, Chang L, Hammock BD, Hashimoto K. Increased expression of soluble epoxide hydrolase in the brain and liver from patients with major psychiatric disorders: A role of brain – liver axis. Journal of Affective Disorders 2020;270:131–4. [PubMed: 32339103]

[25]. Ren Q, Ma M, Yang J, Nonaka R, Yamaguchi A, Ishikawa K-i, et al. Soluble epoxide hydrolase plays a key role in the pathogenesis of Parkinson's disease. Proceedings of the National Academy of Sciences 2018;115:E5815–E23.

[26]. Pu Y, Yang J, Chang L, Qu Y, Wang S, Zhang K, et al. Maternal glyphosate exposure causes autism-like behaviors in offspring through increased expression of soluble epoxide hydrolase. Proceedings of the National Academy of Sciences 2020;117:11753–9.

[27]. Trindade-da-Silva CA, Clemente-Napimoga JT, Abdalla HB, Rosa SM, Ueira-Vieira C, Morisseau C, et al. Soluble epoxide hydrolase inhibitor, TPPU, increases regulatory T cells pathway in an arthritis model. Faseb j 2020;34:9074–86. [PubMed: 32400048]

[28]. Pu Y, Zhang Q, Tang Z, Lu C, Wu L, Zhong Y, et al. Fecal microbiota transplantation from patients with rheumatoid arthritis causes depression-like behaviors in mice through abnormal T cells activation. Translational Psychiatry 2022;12:223. [PubMed: 35650202]

[29]. Zuo Q, Cui W, Liu F, Wang Q, Chen Z, Fan W. Co-cultivated mesenchymal stem cells support chondrocytic differentiation of articular chondrocytes. Int Orthop 2013;37:747–52. [PubMed: 23354690]

[30]. Cheng Y, Si Y, Wang L, Ding M, Yu S, Lu L, et al. The regulation of macrophage polarization by hypoxia-PADI4 coordination in Rheumatoid arthritis. Int Immunopharmacol 2021;99:107988. [PubMed: 34333356]

[31]. Suarez-Arnedo A, Torres Figueroa F, Clavijo C, Arbeláez P, Cruz JC, Muñoz-Camargo C. An image J plugin for the high throughput image analysis of in vitro scratch wound healing assays. PLoS One 2020;15:e0232565. [PubMed: 32722676]

[32]. Pu Y, He Y, Zhao X, Zhang Q, Wen J, Hashimoto K, et al. Depression-like behaviors in mouse model of Sjögren's syndrome: A role of gut-microbiota-brain axis. Pharmacol Biochem Behav 2022;219:173448. [PubMed: 35981685]

[33]. Pu Y, Wu Q, Zhang Q, Huang T, Wen J, Wei L, et al. Mesenchymal stem-cell-derived microvesicles ameliorate MPTP-induced neurotoxicity in mice: a role of the gut–microbiota–brain axis. Psychopharmacology 2023;240:1103–18. [PubMed: 36881113]

[34]. Ding Q, Hu W, Wang R, Yang Q, Zhu M, Li M, et al. Signaling pathways in rheumatoid arthritis: implications for targeted therapy. Signal Transduct Target Ther 2023;8:68. [PubMed: 36797236]

[35]. Liu S, Ma H, Zhang H, Deng C, Xin P. Recent advances on signaling pathways and their inhibitors in rheumatoid arthritis. Clin Immunol 2021;230:108793. [PubMed: 34242749]

[36]. Watanabe S, Alexander M, Misharin AV, Budinger GRS. The role of macrophages in the resolution of inflammation. J Clin Invest 2019;129:2619–28. [PubMed: 31107246]

[37]. Xu Y, Zhang Z, He J, Chen Z. Immune Effects of Macrophages in Rheumatoid Arthritis: A Bibliometric Analysis From 2000 to 2021. Frontiers in Immunology 2022;13.

[38]. Kinne RW, Bräuer R, Stuhlmüller B, Palombo-Kinne E, Burmester GR. Macrophages in rheumatoid arthritis. Arthritis Res 2000;2:189–202. [PubMed: 11094428]

[39]. de Jong TA, Semmelink JF, Denis SW, van de Sande MGH, Houtkooper RHL, van Baarsen LGM. Altered lipid metabolism in synovial fibroblasts of individuals at risk of developing rheumatoid arthritis. Journal of Autoimmunity 2023;134:102974. [PubMed: 36512907]

[40]. Huang W, Zhang L, Cheng C, Shan W, Ma R, Yin Z, et al. Parallel comparison of fibroblast-like synoviocytes from the surgically removed hyperplastic synovial tissues of rheumatoid arthritis and osteoarthritis patients. BMC Musculoskeletal Disorders 2019;20:591. [PubMed: 31812161]

[41]. Bustamante MF, Garcia-Carbonell R, Whisenant KD, Guma M. Fibroblast-like synoviocyte metabolism in the pathogenesis of rheumatoid arthritis. Arthritis Research & Therapy 2017;19:110. [PubMed: 28569176]

[42]. Mahmoud DE, Kaabachi W, Sassi N, Tarhouni L, Rekik S, Jemmali S, et al. The synovial fluid fibroblast-like synoviocyte: A long-neglected piece in the puzzle of rheumatoid arthritis pathogenesis. Frontiers in Immunology 2022;13.

[43]. Bottini N, Firestein GS. Duality of fibroblast-like synoviocytes in RA: passive responders and imprinted aggressors. Nat Rev Rheumatol 2013;9:24–33. [PubMed: 23147896]

[44]. Yoshitomi H Regulation of Immune Responses and Chronic Inflammation by Fibroblast-Like Synoviocytes. Front Immunol 2019;10:1395. [PubMed: 31275325]

[45]. Bergström B, Carlsten H, Ekwall AH. Methotrexate inhibits effects of platelet-derived growth factor and interleukin-1β on rheumatoid arthritis fibroblast-like synoviocytes. Arthritis Res Ther 2018;20:49. [PubMed: 29554943]

[46]. Ma L, Liu H, Chen G, Chen M, Wang L, Zhang X, et al. Sulfasalazine attenuates chronic constriction injury-induced neuroinflammation and mechanical hypersensitivity in rats. Neurosci Lett 2018;683:174–80. [PubMed: 30075286]

[47]. Kim SA, Lee AS, Lee HB, Hur HJ, Lee SH, Sung MJ. Soluble epoxide hydrolase inhibitor, TPPU, attenuates progression of atherosclerotic lesions and vascular smooth muscle cell phenotypic switching. Vascular Pharmacology 2022;145:107086. [PubMed: 35752378]

[48]. Zhang Y, Bai Y, Bai J, Li L, Gao L, Wang F. Targeting Soluble Epoxide Hydrolase with TPPU Alleviates Irradiation-Induced Hyposalivation in Mice via Preventing Apoptosis and Microcirculation Disturbance. Advanced Therapeutics 2020;3:2000115.

[49]. Liang Z, Zhang B, Xu M, Morisseau C, Hwang SH, Hammock BD, et al. 1-Trifluoromethoxyphenyl-3-(1-propionylpiperidin-4-yl) Urea, a Selective and Potent Dual Inhibitor of Soluble Epoxide Hydrolase and p38 Kinase Intervenes in Alzheimer's Signaling in Human Nerve Cells. ACS Chem Neurosci 2019;10:4018–30. [PubMed: 31378059]

[50]. Luo J, Hu S, Fu M, Luo L, Li Y, Li W, et al. Inhibition of soluble epoxide hydrolase alleviates insulin resistance and hypertension via downregulation of SGLT2 in the mouse kidney. J Biol Chem 2021;296:100667. [PubMed: 33864813]

[51]. Yao E-s, Tang Y, Liu X-h, Wang M-h. TPPU protects tau from H2O2-induced hyperphosphorylation in HEK293/tau cells by regulating PI3K/AKT/GSK-3β pathway. Journal of Huazhong University of Science and Technology [Medical Sciences] 2016;36:785–90. [PubMed: 27924507]

[52]. Borsini A The role of soluble epoxide hydrolase and its inhibitors in depression. Brain, Behavior, & Immunity - Health 2021;16:100325.

[53]. Minaz N, Razdan R, Hammock BD, Goswami SK. An inhibitor of soluble epoxide hydrolase ameliorates diabetes-induced learning and memory impairment in rats. Prostaglandins Other Lipid Mediat 2018;136:84–9. [PubMed: 29751149]

[54]. Luo A, Wu Z, Li S, McReynolds CB, Wang D, Liu H, et al. The soluble epoxide hydrolase inhibitor TPPU improves comorbidity of chronic pain and depression via the AHR and TSPO signaling. J Transl Med 2023;21:71. [PubMed: 36732752]

[55]. Atone J, Wagner K, Hashimoto K, Hammock BD. Cytochrome P450 derived epoxidized fatty acids as a therapeutic tool against neuroinflammatory diseases. Prostaglandins Other Lipid Mediat 2020;147:106385. [PubMed: 31698143]

[56]. McReynolds CB, Cortes-Puch I, Ravindran R, Khan IH, Hammock BG, Shih PB, et al. Plasma Linoleate Diols Are Potential Biomarkers for Severe COVID-19 Infections. Front Physiol 2021;12:663869. [PubMed: 33868029]

[57]. Bergmann CB, McReynolds CB, Wan D, Singh N, Goetzman H, Caldwell CC, et al. sEH-derived metabolites of linoleic acid drive pathologic inflammation while impairing key innate immune cell function in burn injury. Proc Natl Acad Sci U S A 2022;119:e2120691119. [PubMed: 35312372]

[58]. Nagatake T, Shiogama Y, Inoue A, Kikuta J, Honda T, Tiwari P, et al. The 17,18-epoxyeicosatetraenoic acid-G protein-coupled receptor 40 axis ameliorates contact hypersensitivity by inhibiting neutrophil mobility in mice and cynomolgus macaques. J Allergy Clin Immunol 2018;142:470–84.e12. [PubMed: 29288079]

[59]. Cashman JR, Hanks D, Weiner RI. Epoxy derivatives of arachidonic acid are potent stimulators of prolactin secretion. Neuroendocrinology 1987;46:246–51. [PubMed: 3658112]

[60]. Morin C, Sirois M, Echavé V, Albadine R, Rousseau E. 17,18-epoxyeicosatetraenoic acid targets PPARγ and p38 mitogen-activated protein kinase to mediate its anti-inflammatory effects in the lung: role of soluble epoxide hydrolase. Am J Respir Cell Mol Biol 2010;43:564–75. [PubMed: 20008283]

[61]. Hara S, Tojima I, Shimizu S, Kouzaki H, Shimizu T. 17,18-Epoxyeicosatetraenoic Acid Inhibits TNF-α-Induced Inflammation in Cultured Human Airway Epithelium and LPS-Induced Murine Airway Inflammation. Am J Rhinol Allergy 2022;36:106–14. [PubMed: 34236247]

[62]. Cutolo M, Soldano S, Gotelli E, Montagna P, Campitiello R, Paolino S, et al. CTLA4-Ig treatment induces M1–M2 shift in cultured monocyte-derived macrophages from healthy subjects and rheumatoid arthritis patients. Arthritis Research & Therapy 2021;23:306. [PubMed: 34952630]

[63]. Tardito S, Martinelli G, Soldano S, Paolino S, Pacini G, Patane M, et al. Macrophage M1/M2 polarization and rheumatoid arthritis: A systematic review. Autoimmunity Reviews 2019;18:102397. [PubMed: 31520798]

[64]. Chen Z, Tang Y, Yu J, Dong R, Yang Y, Fu M, et al. sEH Inhibitor Tppu Ameliorates Cecal Ligation and Puncture-Induced Sepsis by Regulating Macrophage Functions. Shock 2020;53:761–71. [PubMed: 31318834]

[65]. Zhang J, Zhang M, Huo X-K, Ning J, Yu Z-L, Morisseau C, et al. Macrophage Inactivation by Small Molecule Wedelolactone via Targeting sEH for the Treatment of LPS-Induced Acute Lung Injury. ACS Central Science 2023;9:440–56. [PubMed: 36968547]

[66]. Lee GR. The Balance of Th17 versus Treg Cells in Autoimmunity. Int J Mol Sci 2018;19. [PubMed: 30577572]

[67]. Yan JB, Luo MM, Chen ZY, He BH. The Function and Role of the Th17/Treg Cell Balance in Inflammatory Bowel Disease. J Immunol Res 2020;2020:8813558. [PubMed: 33381606]

[68]. Zhang S, Gang X, Yang S, Cui M, Sun L, Li Z, et al. The Alterations in and the Role of the Th17/Treg Balance in Metabolic Diseases. Frontiers in Immunology 2021;12.

[69]. Yang J, Bratt J, Franzi L, Liu JY, Zhang G, Zeki AA, et al. Soluble epoxide hydrolase inhibitor attenuates inflammation and airway hyperresponsiveness in mice. Am J Respir Cell Mol Biol 2015;52:46–55. [PubMed: 24922186]

[70]. Tian Y, Yuan X, Wang Y, Wu Q, Fang Y, Zhu Z, et al. Soluble epoxide hydrolase inhibitor attenuates BBB disruption and neuroinflammation after intracerebral hemorrhage in mice. Neurochem Int 2021;150:105197. [PubMed: 34592333]

[71]. Chen S, Saeed A, Liu Q, Jiang Q, Xu H, Xiao GG, et al. Macrophages in immunoregulation and therapeutics. Signal Transduct Target Ther 2023;8:207. [PubMed: 37211559]

[72]. Chen Y, Tian H, Yao E, Tian Y, Zhang H, Xu L, et al. Soluble epoxide hydrolase inhibition Promotes White Matter Integrity and Long-Term Functional Recovery after chronic hypoperfusion in mice. Sci Rep 2017;7:7758. [PubMed: 28798352]

[73]. Di Giuseppe D, Discacciati A, Orsini N, Wolk A. Cigarette smoking and risk of rheumatoid arthritis: a dose-response meta-analysis. Arthritis Res Ther 2014;16:R61. [PubMed: 24594022]

[74]. Hammock BD, McReynolds CB, Wagner K, Buckpitt A, Cortes-Puch I, Croston G, et al. Movement to the Clinic of Soluble Epoxide Hydrolase Inhibitor EC5026 as an Analgesic for Neuropathic Pain and for Use as a Nonaddictive Opioid Alternative. Journal of Medicinal Chemistry 2021;64:1856–72. [PubMed: 33550801]

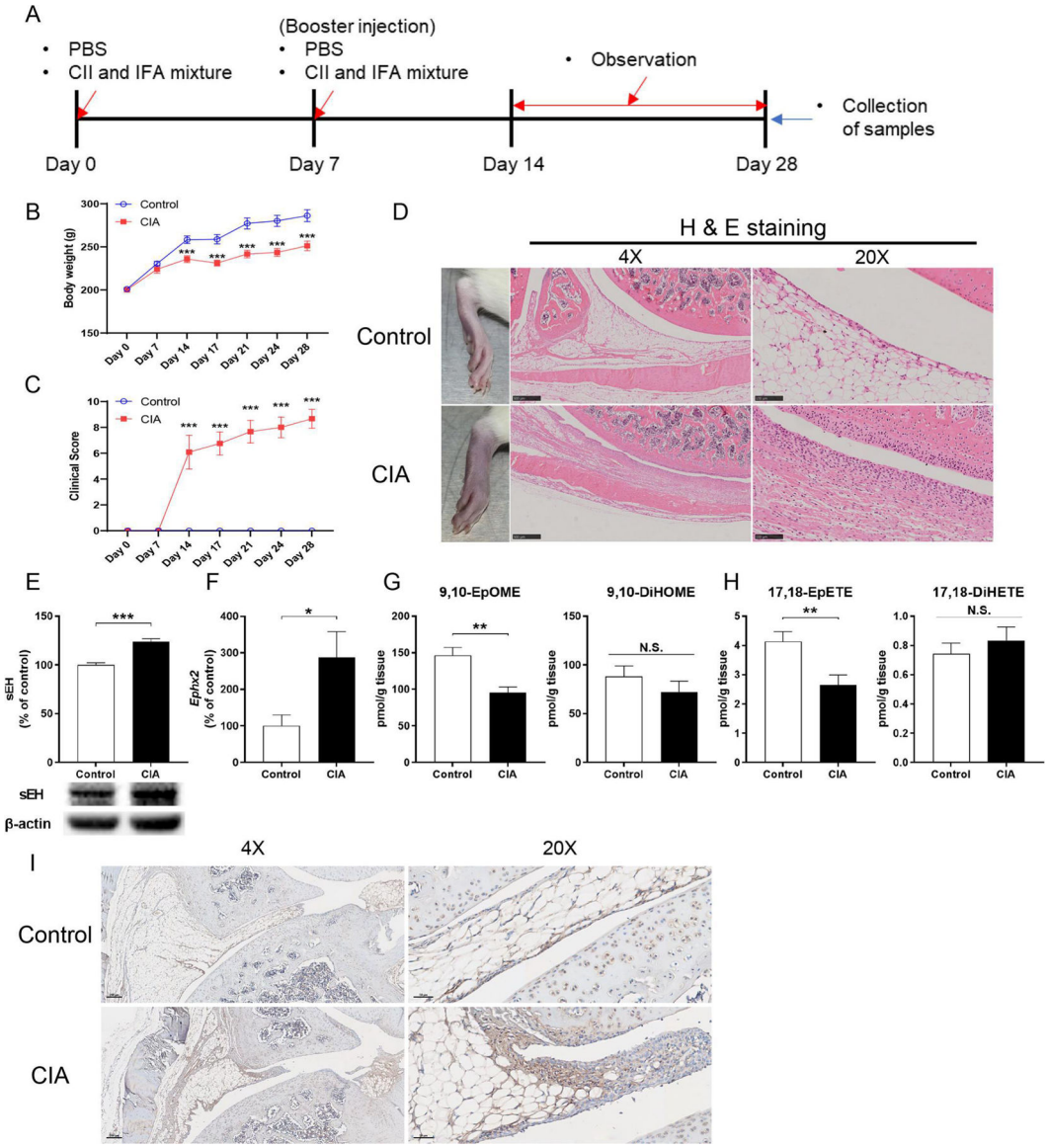

Figure 1. Increased expression of sEH and decreased EpFAs in the joint of CIA rats

(A): Schedule of treatment and sample collection. (B): Change of body weight of the rats. (C): Change of clinical score of control and CIA rats. (D): H&E staining of the joint from two groups of rats. (E): Protein expression of sEH in the joint of rats. (F): Gene expression of *Ephx2* mRNA in the joint of rats. (G): Levels of 9,10-EpOME and 9,10-DiHOME in the joint of control and CIA rats. (H): Levels of 17,18-EpETE and 17,18-DiHETE in the joint of control and CIA rats. (I): Representative images of sEH immunohistochemistry in synovial tissues. The values represent the mean ± SEM (n = 10). *P < 0.05, **P < 0.01, ***P < 0.001 compared to the control group by Student t-test.

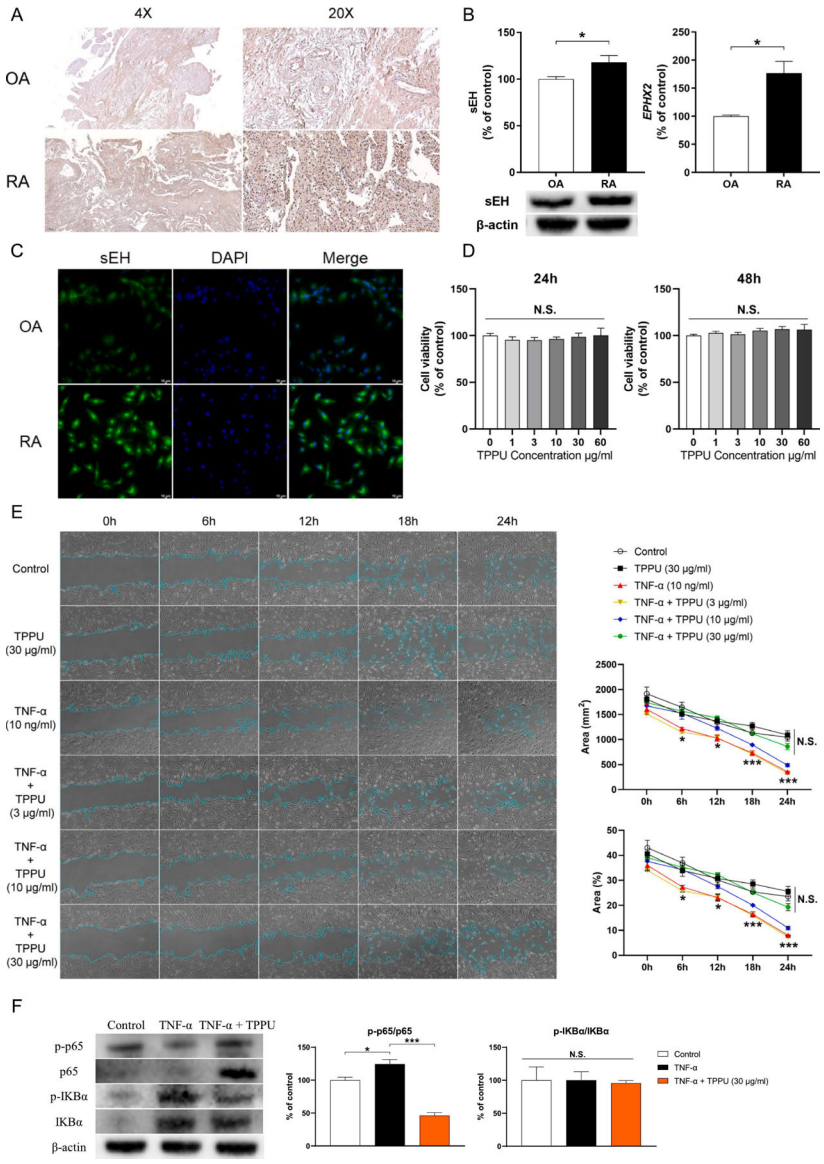

Figure 2. Increased expression of sEH in the FLS from RA patients and effects of TPPU

(A): Representative images of sEH immunohistochemistry in synovial tissues from RA patients and OA patients (n = 5). (B): Protein expression of sEH and gene expression of *Ephx2* mRNA in the fibroblast-like synoviocytes (FLS) from RA and OA patients. (C): Representative images of sEH immunofluorescence in FLS from RA patients and OA patients. (D): Effects of TPPU on cell viability in the FLS from RA patients. (E): Effects of TPPU on wound healing assay in the FLS from RA patients. (F): Effects of TPPU on the expression of p65, p-p65 and IkB in the FLS from RA patients. All cell experiments were triplicated from different patients. Data are shown as mean ± SEM (n = 3). *P <0.05, **P <0.01, ***P <0.001, N.S., not significant.

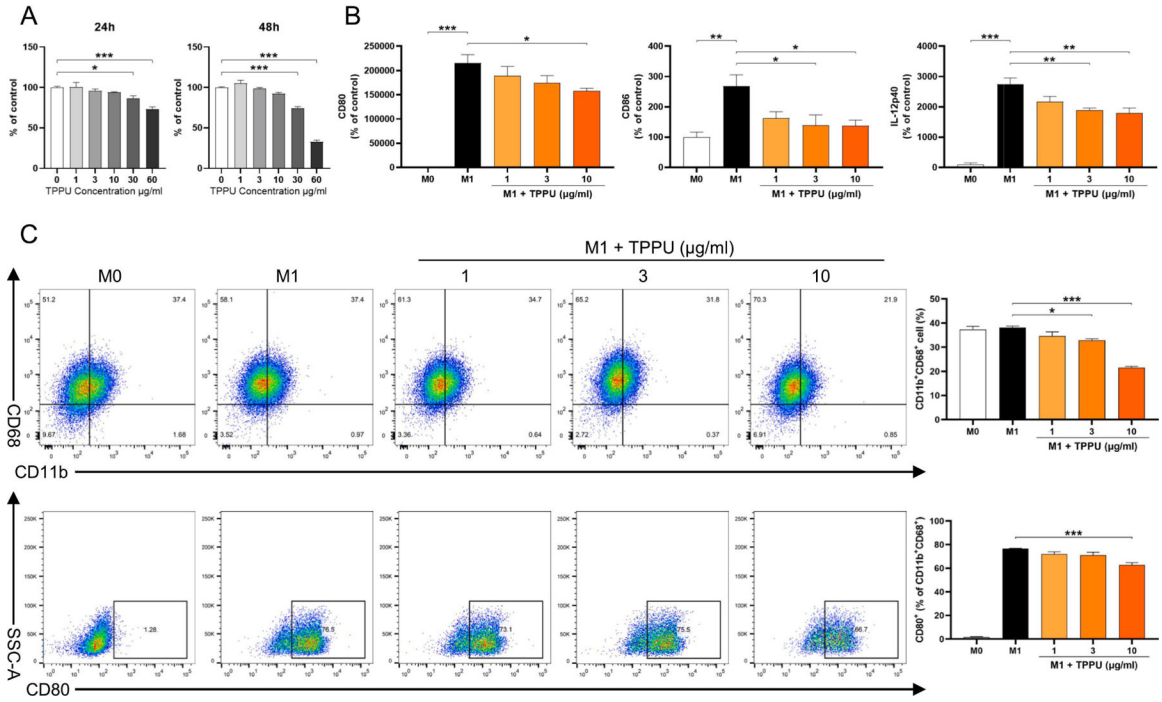

Figure 3. Effects of TPPU on the polarization of Thp-1-derived macrophages

(A): Effects of TPPU on cell viability in the Thp-1 cells. (B): RT-PCR analysis of M1 macrophages markers of CD80, CD86 and IL-12p40. (C): Representative images of different expression of macrophages ($CD11b^+CD68^+$ cells, % of total cells) and M1 polarized macrophages ($CD80^+$ cells, % of $CD11b^+CD68^+$ cells). All experiments were triplicated from different cell lines. Data are shown as mean ± SEM (n = 3). *P <0.05, **P <0.01, ***P <0.001.

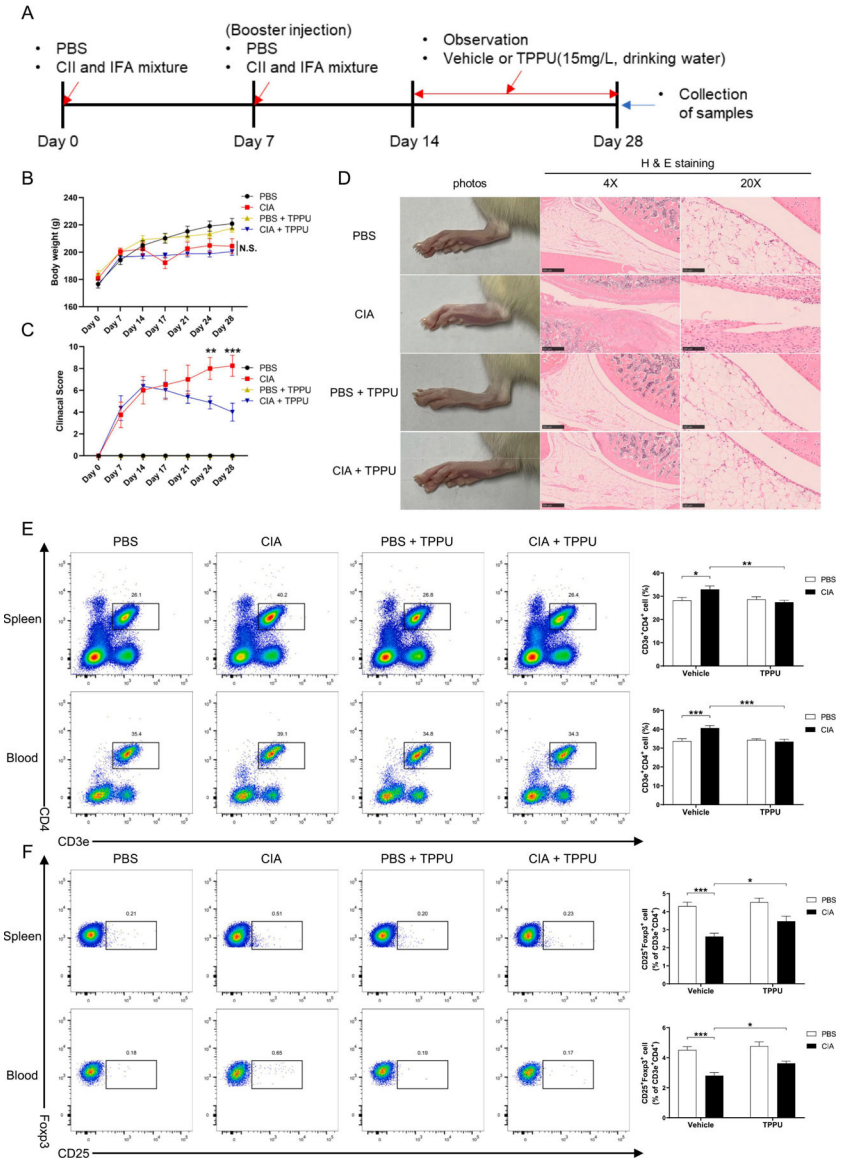

Figure 4. Effects of TPPU on joint inflammation and T cell immune activation of CIA rats

(A): Schedule of treatment and sample collection. (B): Change of body weight of the rats among the four groups. (C): Change of clinical score of the four groups of rats. (D): Representative photos and H&E staining of the joint from four groups of rats. (E): Representative images of different expression of $CD3e^{+}CD4^{+}$ cells (% of total cells) in spleen and blood of the four groups of rats. (F): Representative images of different expression of Treg cells ($CD25^{+}Foxp3^{+}$ cells, % of $CD3e^{+}CD4^{+}$ T cell) in spleen and blood of the four groups of rats. Data are shown as mean ± SEM (n = 8). *P <0.05, **P <0.01, ***P <0.001, N.S., not significant.